Properties of Solar Wind Dynamic Pressure Pulses at 1 AU during the Deep Minimum between Solar Cycles 23 and 24

Y. Q. Xie, P. B. Zuo, X. S. Feng & Y. Zhang

Solar Physics
A Journal for Solar and Solar-Stellar Research and the Study of Solar Terrestrial Physics

ISSN 0038-0938
Volume 290
Number 6

Sol Phys (2015) 290:1835-1849
DOI 10.1007/s11207-015-0700-5

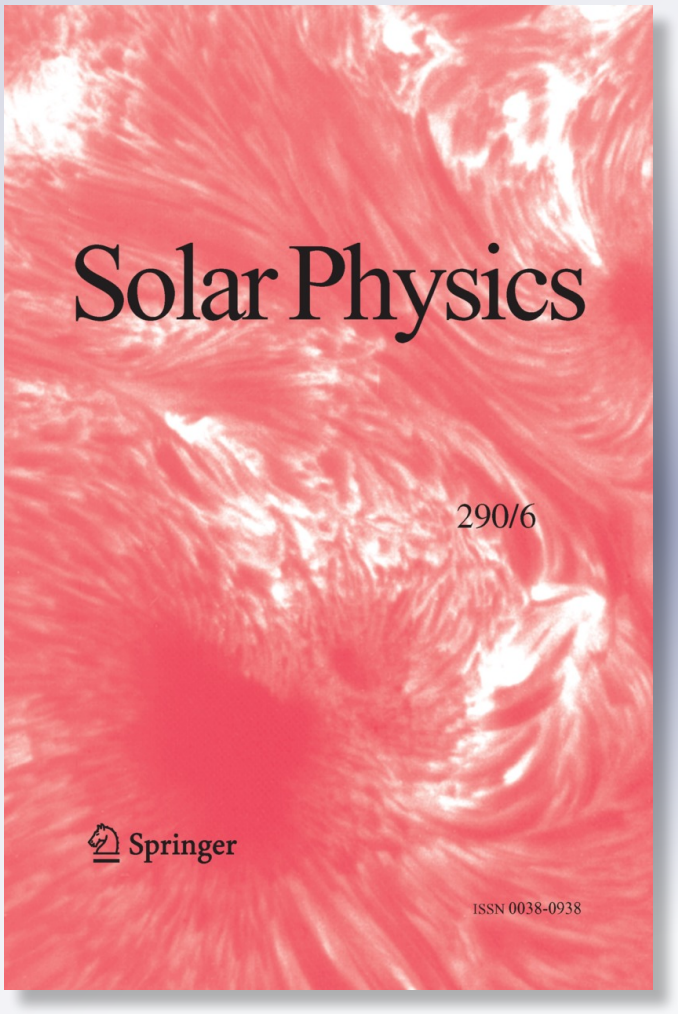

Springer

Solar Phys (2015) 290:1835–1849
DOI 10.1007/s11207-015-0700-5

Properties of Solar Wind Dynamic Pressure Pulses at 1 AU during the Deep Minimum between Solar Cycles 23 and 24

Y.Q. Xie[1] · P.B. Zuo[2] · X.S. Feng[2] · Y. Zhang[1]

Received: 28 September 2014 / Accepted: 6 May 2015 / Published online: 21 May 2015

Abstract Observations during the deep solar minimum between Solar Cycles 23 and 24 offer an opportunity for characterizing the nature of solar wind dynamic pressure pulses (DPPs) under extreme solar activity. In this study, we identify 226 DPPs from July 2008 to June 2009 using an automatic detection algorithm based on high-resolution plasma data from the *Wind* spacecraft to investigate the features of DPPs during the deep solar minimum. For comparison, the similarities and differences of the statistical characteristics of the DPPs during the deep solar minimum and during the previous solar minimum are also examined. It is found that the number and the occurrence rate of DPPs during the deep solar minimum are only about one-third of those during the previous minimum, which may be attributed to lower solar wind dynamic pressure and weaker dynamic pressure fluctuations. From a statistical perspective, however, no obvious difference is apparent between the other basic DPP properties in the two solar minima, such as the absolute and relative amplitude of the dynamic pressure changes and the durations of the transition regions of DPPs. Other basic properties of the DPPs during the deep solar minimum are as follows: 1) the distribution of the absolute value of the dynamic pressure amplitude change peaks at 1.0 – 1.5 nPa, 2) the most probable relative pressure changes are 0.2 – 0.8, 3) DPP durations are broad-peaked between 150 s and 210 s with a mean of about 171 s, 4) 76.7 % of the DPPs can be considered as pressure balance structures, 5) dynamic pressure changes across DPPs are dominated by density changes, 6) specially, during the deep solar minimum, a considerable portion of DPPs, 86.7 %, are associated with large-scale solar wind transients such as interplanetary coronal mass ejections (ICMEs) and stream interaction regions (SIRs).

Keywords Solar wind dynamic pressure pulse · The deep solar minimum · Pressure balance structure · Large-scale solar wind transient

✉ P.B. Zuo
pbzuo@spaceweather.ac.cn

1 College of Meteorology and Oceanography, PLA University of Science and Technology, Nanjing, China

2 State Key Laboratory of Space Weather, National Space Science Center, Chinese Academy of Sciences, Beijing, China

1. Introduction

In the solar wind, small-scale plasma structures with sharp (*i.e.*, with steep fronts) and large changes (in amplitude) of solar wind dynamic pressure are frequently observed. These structures are often called solar wind dynamic pressure pulses (DPPs) when there are only small variations in their preceding and succeeding regions. The time scale of the dynamic pressure front of DPPs ranges from a few seconds to several minutes (Dalin *et al.*, 2002). Moreover, abrupt changes of solar wind dynamic pressure are generally accomplished by sharp variations of ion flux (Riazantseva *et al.*, 2003b; Zastenker and Riazantseva, 2007).

Usually the strong DPPs with large amplitude changes of dynamic pressure may compress the Earth's magnetosphere intensively and have significant effects on the magnetosphere-ionosphere coupling system (*e.g.* Borodkova *et al.*, 2005; Parkhomov, Riazantseva, and Zastenker, 2005; Moore *et al.*, 2007; Motoba *et al.*, 2007; Yu and Ridley, 2011). Numerous studies have discussed the responses of this system to large DPPs and their potential space weather effects. On the other hand, the occurrence of sharp solar wind plasma and magnetic field changes is often associated with fundamental physical processes, such as plasma instability (Dalin *et al.*, 2002; Riazantseva *et al.*, 2005b), magnetic turbulence (Riazantseva *et al.*, 2007), magnetic reconnection (Khabarova and Zastenker, 2011), or interactions between different kinds of solar wind streams (Riazantseva *et al.*, 2003a). Further study of DPPs can lead to a better understanding of the nature of solar wind plasma.

The unusual solar minimum between Solar Cycles 23 and 24, from mid-2007 to mid-2009, created a record number of spotless days over several recent solar cycles (Gibson *et al.*, 2009; Jian, Russell, and Luhmann, 2011). A number of studies have documented the characteristics of the solar-heliospheric-geospace system during the period of this deep solar minimum, with a focus on solar activity abnormalities (Russell, Jian, and Luhmann, 2013; Solomon *et al.*, 2010; Chen, Liu, and Wan, 2011), unprecedented solar wind and interplanetary conditions (Jian, Russell, and Luhmann, 2011; Kilpua *et al.*, 2012), and their consequences in the geospace (*e.g.* Heelis *et al.*, 2009; Emmert, Lean, and Picone, 2010; Lühr and Xiong, 2010; Solomon *et al.* 2010, 2011; Araujo-Pradere *et al.*, 2011; Liu *et al.* 2011, 2012). In this study, we attempt to characterize the properties of DPPs during this deep solar minimum using high-resolution plasma data from the *Wind* spacecraft to enrich our understanding of the solar wind plasma during extremely low solar activity. Here we select July 2008 – June 2009 to represent the period of deep minimum occurring between Solar Cycles 23 and 24 because the lowest number of sunspots is reported during this 1-year interval (Jian, Russell, and Luhmann, 2011). For comparison, we also investigate the DPPs identified during the whole year of 1996, which is taken to represent the period of the previous solar minimum. In the following sections, we first describe the criteria and detection method for identification of DPP events, and then present the results of our statistical and comparative investigation. The difference and similarity of the statistical characteristics of the DPPs during the two recent solar minima are discussed in Section 4. In the last section, a brief summary is given.

2. Selection Criteria for DPPs

We inspect *Wind* solar wind plasma data to detect abrupt changes of the solar wind dynamic pressure, $P_{dy} = m_p N_p V_p^2$, where m_p is the proton mass, N_p is the plasma density,

and V_p is the solar wind bulk speed. The solar wind plasma and magnetic field data are obtained from the *Three-Dimensional Plasma and Energetic Particle Investigation* (3DP) and the *Magnetic Field Investigation* (MFI) instruments on board the *Wind* spacecraft with a time resolution as high as 3 seconds (ftp://cdaweb.gsfc.nasa.gov/pub/data/wind/3dp/; ftp://cdaweb.gsfc.nasa.gov/pub/data/wind/mfi/).

The selection of the DPP events in this study is guided by the following criteria: 1) Solar wind dynamic pressure changes by at least 1 nPa in less than 5 min. 2) The structure with increased or decreased solar wind dynamic pressure should be isolated in the sense that only small variations in solar wind dynamic pressure occur in the preceding and succeeding three minutes. Since the data resolution is very high, the three-minute intervals can be considered representative of the status before and after the pressure front. The relatively quiet regions are called upstream and downstream. In the upstream and downstream regions, the ratio of the standard deviation of the dynamic pressure to the average dynamic pressure should be less than 0.6. 3) The change in the amplitude of the dynamic pressure in the upstream region and in the downstream region is less than 0.6 times the change in its amplitude in the transition region. 4) There are times with gaps between the region of abrupt change in the dynamic pressure (which is usually named the transition region) and the upstream and downstream regions, especially for complex structures (see Figures 1b and 1d). The duration of the gap should be less than 180 s.

The candidate DPPs are firstly selected by an automated detection algorithm developed using the criteria mentioned above from the corresponding *Wind*/3DP datasets (Zuo *et al.*, 2015). The automatically identified events are then re-examined visually. In this step, events with invalid 3DP data are excluded, and, if necessary, regions of DPPs and their upstream and downstream regions are further adjusted. This two-step verification makes us confident in the identification process.

DPPs can be classified into two categories according to the change of sign of the solar wind dynamic pressure across the transition region: a positive change indicates increased dynamic pressure, while a negative change signifies decreased dynamic pressure. Figures 1a and b show two examples of positive DPPs, and 1c and d of negative ones. The first four panels in each subfigure are the magnetic field magnitude (B_t) and the three components of the magnetic field (B_x, B_y, B_z) in Geocentric Solar Magnetospheric (GSM) coordinates, respectively. In the following panels, T_p is the proton temperature, N_p is the proton number density, V_p is the solar wind speed, and P_{dy} is the solar wind dynamic pressure in units of nPa. The solid red vertical lines in the figures indicate the identified boundaries of the transition region. The upstream and downstream regions of the DPP are marked by transverse lines before and after the DPP. The isolated upstream and downstream regions are relatively quiet. The figure also indicates that sudden pressure changes are usually accomplished by abrupt changes in magnetic field magnitude and direction.

3. Statistical Results

During the deep solar minimum from 1 July 2008 to 30 June 2009, 226 DPPs were identified with our automatic detection code. The analysis below is based on these events. On average, the occurrence rate of DPPs is 0.7 events *per* day during this period. The number of DPPs detected each day is presented as a histogram in Figure 2. The red and green bars below the abscissa mark the dates during which interplanetary coronal mass ejections (ICMEs) and stream interaction regions (SIRs) were observed (these will be addressed in Section 3.3).

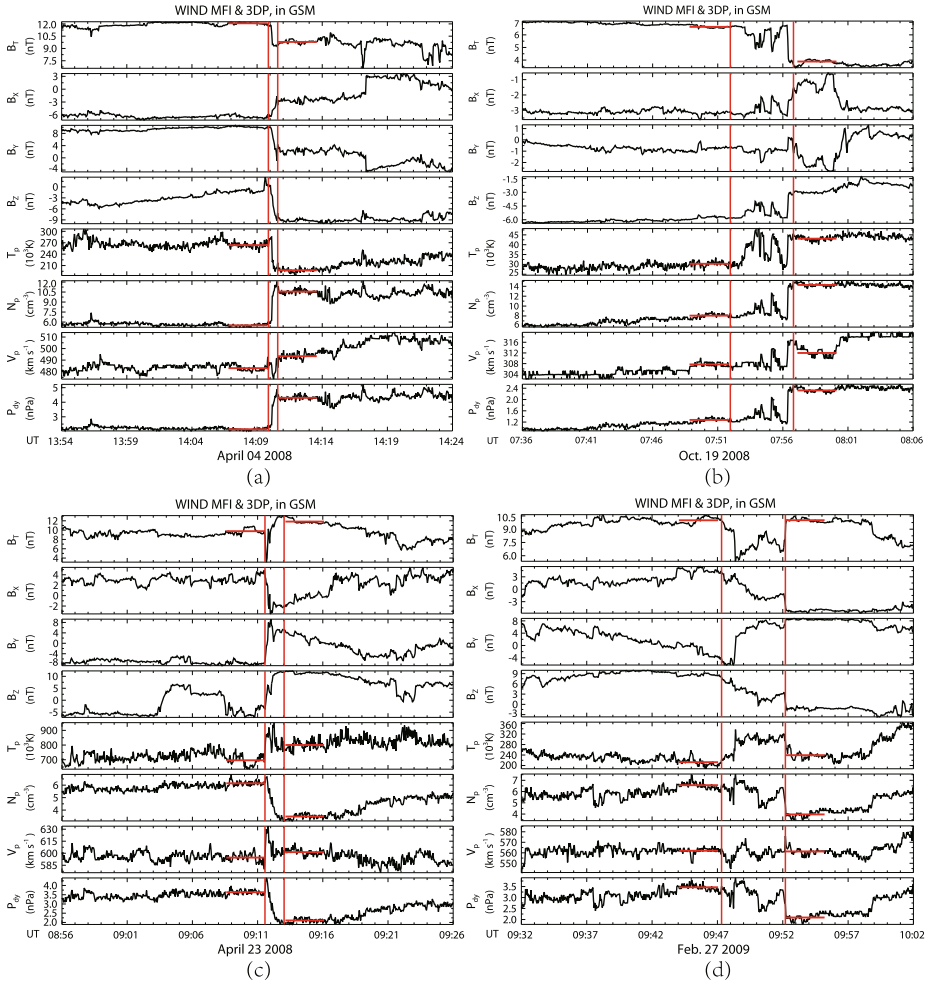

Figure 1 Examples of positive-type ((a) and (b)) and negative-type ((c) and (d)) DPP events detected by *Wind*. From top to bottom: magnetic field strength, the three components (x, y, z) of the magnetic field in Geocentric Solar Magnetospheric (GSM) coordinates, proton temperature, proton density, solar wind speed, and solar wind dynamic pressure. Solid red vertical lines indicate boundaries of the DPP events, transverse lines before and after the DPPs mark the upstream and downstream regions.

In addition, there are some gaps in the 3DP data during this period. Here, dates with data gaps are shown in the figure by black blocks at its top. DPPs are not distributed homogeneously but appear in groups. DPPs are observed during only 19.6 % of the observational period.

For comparison, we also identify DPPs during 1996 using the same criteria and algorithm. We detect a total of 732 DPPs during 366 observational days with a frequency of 2.0 DPP events *per* day. The average occurrence frequency of DPPs during the deep solar minimum is about one-third of that observed during the previous minimum. The significant difference between the two solar minima may be attributed to different background solar wind conditions. We will discuss this point in Section 4.

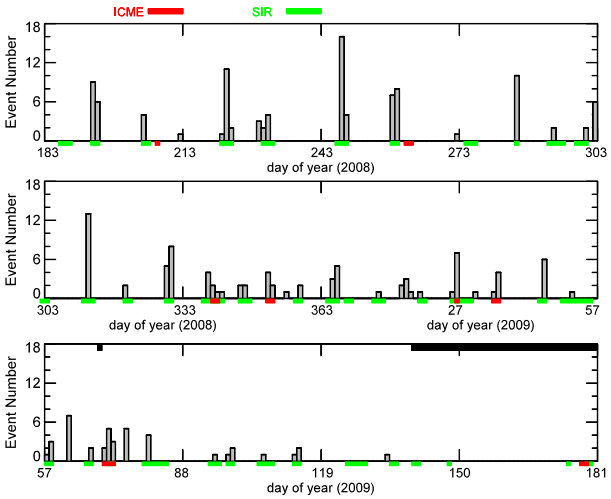

Figure 2 Number of DPPs *per* day during the deep solar minimum occurring from 1 July 2008 to 30 June 2009. In each panel, the red and green bars below the abscissa denote the dates in which ICMEs (red) and SIRs (green) were observed. Black blocks at the top mark periods without valid *Wind*/3DP data.

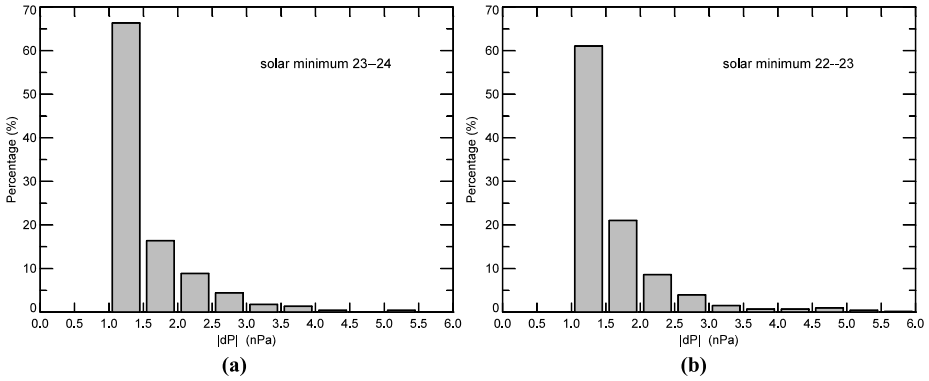

Figure 3 Distributions of absolute dynamic pressure changes. (a) Histogram for the solar minimum between Cycles 23 and 24 and (b) for the solar minimum between Cycles 22 and 23.

3.1. Basic Properties

3.1.1. Distribution of the Dynamic Pressure Amplitude Change across the DPPs

The distribution of the absolute value of the dynamic pressure amplitude change across the DPPs, $|dP|$, is presented as a histogram in Figure 3, where the bin interval is set to be 0.5 nPa. The value of $|dP|$ for the events during the deep solar minimum varies from 1.0 nPa to 5.07 nPa with an average value of 1.52 nPa. As seen from Figure 3a, the distribution of $|dP|$ peaks at 1.0 – 1.5 nPa and the pressure changes in about 66.4 % of the cases are in this range. Only very few events are located in the bins between 4.5 nPa and 6.0 nPa. For the previous solar minimum (Figure 3b), the $|dP|$ of all 732 cases varies from 1.0 nPa to 12.74 nPa with an average value of 1.64 nPa which is about 8 % larger than that for the deep minimum. A comparison between the two solar minima suggests little difference in the distributions. However, it is noteworthy that there are less strong DPPs during the deep solar minimum than during the previous one. During the solar minimum between Cycles 22

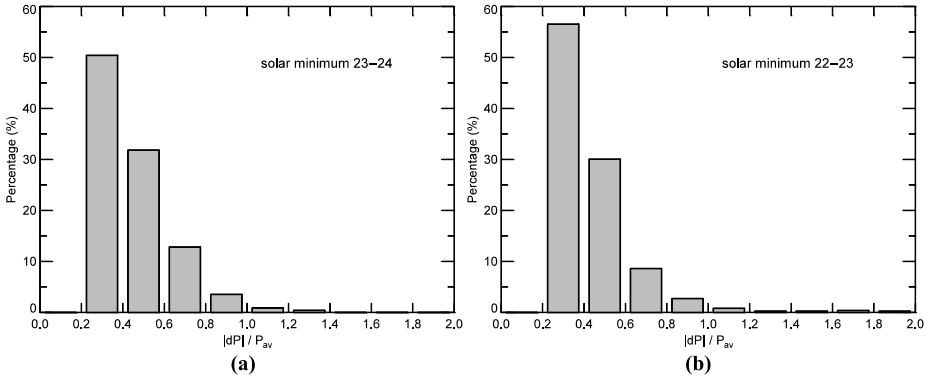

Figure 4 Distributions of the relative pressure changes. (a) Histogram for the solar minimum between Cycles 23 and 24 and (b) for the solar minimum between Cycles 22 and 23.

and 23, $|dP|$ is greater than 3 nPa and 6 nPa in 39 and seven cases (not shown in Figure 3b), respectively. While during the minimum between Cycles 23 and 24, $|dP|$ is in all cases lower than 6 nPa; only nine cases have $|dP|$ values greater than 3 nPa.

Figure 4 shows the distribution of the ratio of the absolute value of the pressure change ($|dP|$) to the average dynamic pressure strength ($P_{\rm av}$), $|dP|/P_{\rm av}$, where $P_{\rm av} = (P_1 + P_2)/2$, and P_1 and P_2 are the averages of the dynamic pressure in the upstream and downstream of the DPP, respectively. This relative value determines the strength of the DPP compared with the background condition it resides in. The most probable relative pressure changes during the deep solar minimum are 0.2 – 0.8 (see Figure 4a). The value of $|dP|/P_{\rm av}$ for all 226 cases varies from 0.20 to 1.21 with an average value of 0.44. In about 95.1 % of these DPPs, $|dP|/P_{\rm av}$ is in the range of 0.2 to 0.8; 1.3 % of the events have $|dP|/P_{\rm av}$ values greater than 1. The distribution of $|dP|/P_{\rm av}$ for DPPs during the solar minimum between Cycles 22 and 23 is similar to that of the deep solar minimum, as shown in Figure 4b. The $|dP|/P_{\rm av}$ of all 732 cases during 1996 varies from 0.20 to 1.98 with an average of 0.43. In about 95.2 % of the 732 events, $|dP|/P_{\rm av}$ is in the range of 0.2 to 0.8; about 2.0 % of the events have $|dP|/P_{\rm av}$ values greater than 1.

3.1.2. Relationship between the Relative Pressure Changes and the Relative Density Changes

Dalin *et al.* (2002) surveyed DPPs using nearly 3 years of high-time resolution solar wind data from the *Interball-1* (1996 and 1998) and the *Interplanetary Monitoring Platform 8* (IMP 8) (1979). The authors concluded that the dynamic pressure changes for DPPs resulted mainly from density changes. In this article, we investigate this issue using *Wind* high-resolution observations of the deep solar minimum. Relative pressure changes ($dP/P_{\rm av}$) are compared with relative density changes ($dN/N_{\rm av}$), where dN is the change of density across the DPPs, and $N_{\rm av} = (N_1 + N_2)/2$, where N_1 and N_2 are the density averages in the upstream and downstream of the DPP, respectively. As can be seen in Figure 5, almost all of the 226 data points are close to the line with slope equal to 1. Furthermore, the correlation coefficient of this linear fit is 0.99, and the average value of the ratio $(dP/P_{\rm av})/(dN/N_{\rm av})$ is 1.13. Similarly, for the events during the solar minimum between Cycles 22 and 23, the corresponding correlation coefficient and average value are 0.98 and 1.15, respectively.

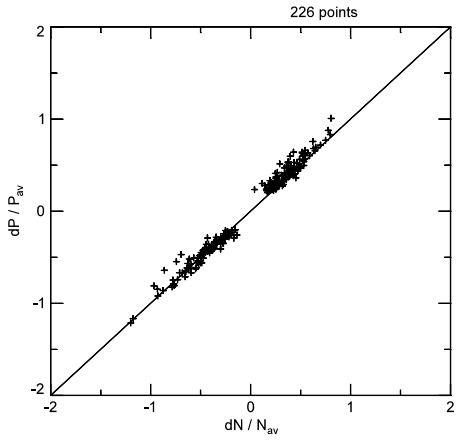

Figure 5 The relative pressure changes in function of the relative density changes.

In addition, the velocity changes across the DPPs are generally small, with the exception of a few interplanetary (IP) shocks (only nine cases of all 226 DPPs are identified as IP shocks). During the deep solar minimum, the average value of the velocity changes is only about 12 km s^{-1}, which is close to the 13 km s^{-1} of the previous solar minimum. Almost all of the 226 events, about 98.2 %, are accompanied by very small changes (below 50 km s^{-1}) in solar wind velocity. Therefore, our results confirm that the dynamic pressure changes during the deep solar minimum and the previous solar minimum are dominated by density changes and that the role of velocity changes is rather small.

3.1.3. Transition Region Durations

The distribution of the durations of the transition regions, dT, is shown in Figure 6a for the 226 cases during the deep solar minimum. According to the restrictions imposed by our selection criteria, all of the events have maximum duration of 300 s. Overall, the distribution has a broad peak between 150 s and 210 s with a mean of 171 s and a minimum duration of 3 s, which is the time resolution of the data. A large number of events, 73.5 %, have durations greater than 120 s; only 26.5 % have durations less than 120 s. Very sharp changes of less than 10 s are detected in only 2.2 % of the events (five cases).

As shown in Figure 6b, the statistic results of DPP durations during the solar minimum between Cycles 22 and 23 are similar to those recorded during the deep solar minimum. In the previous minimum, the average duration is 173 s, and the most probable value of the transition time is 150 – 240 s. About 23.9 % of the observed pressure fronts have transition times of less than 120 s; about 1 % of the events have transition times of less than 10 s.

A comparison of the durations of pressure changes (dT) and their amplitudes ($|dP|$) shows no clear relationship, or in other words, the amplitudes and transition times of the pressure changes are independent (not shown). This conclusion is in agreement with that of Dalin *et al.* (2002). The relationship between the absolute values of the pressure changes and their transition times is presented in Table 1. In this table, the number of observed events is listed as a function of $|dP|$ and dT. The core of the event distribution, 91 of the 226 cases, have a transition time > 180 s and absolute pressure changes of 1 nPa to 2 nPa. In general, the largest pressure changes are not the fastest ones.

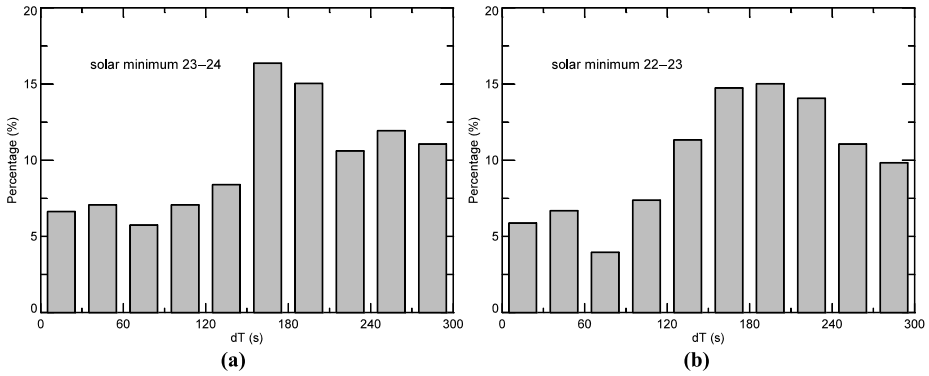

Figure 6 Distribution of the durations of DPPs. (a) Histogram for the solar minimum between Cycles 23 and 24 and (b) for the solar minimum between Cycles 22 and 23.

Table 1 Distribution of the absolute value of the dynamic pressure amplitude change $|dP|$ (in nPa) and the duration of the transition region dT (in seconds) during the deep minimum.

$\|dP\|$ [nPa]	dT [s]			
	<10	10 – 60	60 – 180	>180
1 – 2	4	23	69	91
2 – 4	1	3	16	17
>4	0	0	0	2

3.2. Pressure Balance Analysis

It is important to determine whether the total pressure is in balance across the observed sharp pressure changes because this balance affects the time evolution of small-scale solar wind structures (Barkhatov *et al.*, 2003).

A comparison of thermal and magnetic pressure changes is presented in Figure 7, where $dP_{\rm th}$ ($dP_{\rm th} = P_{\rm th2} - P_{\rm th1}$) denotes the thermal pressure change, and $P_{\rm th1}$ and $P_{\rm th2}$ represent the thermal pressures before and after the event, respectively. Similarly, $dP_{\rm m} = P_{\rm m2} - P_{\rm m1}$ denotes magnetic pressure change, with $P_{\rm m1}$ and $P_{\rm m2}$ representing the magnetic pressures before and after the pressure front, respectively. In 92.0 % of 224 cases (for two cases,

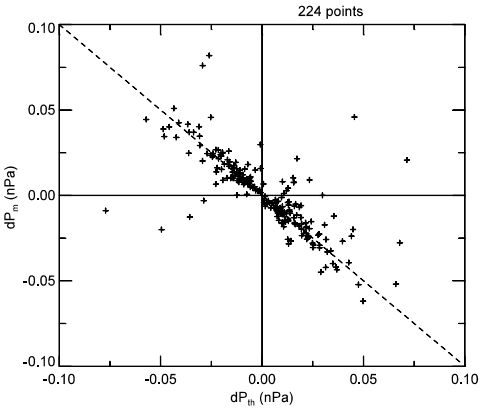

Figure 7 Solar wind magnetic pressure change ($dP_{\rm m}$) plotted against the thermal pressure change ($dP_{\rm th}$) for each case. The dashed line has a slope equal to 1.

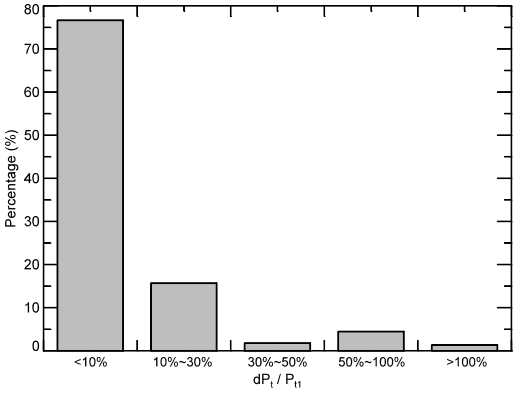

Figure 8 Histogram of solar wind relative total pressure changes dP_t/P_{t1} across the boundaries of the DPPs.

no valid data are available), the changes in the thermal and magnetic field pressure have the opposite sign, as required for pressure balance, with an increase in thermal pressure coinciding with a decrease in magnetic pressure and *vice versa*. Although these changes are significant for maintaining pressure balance, we check the conservation of the total pressure balance quantitatively by comparing the sum of the thermal and magnetic pressures on each side of the DPP.

We calculate the total pressure ($P_t = P_{th} + P_m$, where P_{th} is thermal pressure and P_m is magnetic pressure) as the sum of proton thermal pressure, electron thermal pressure, α particle thermal pressure, and magnetic pressure. The calculation is performed using the solar wind measurements of proton density (N_i), electron density (N_e), α particle density (N_α), proton temperature (T_i), electron temperature (T_e), α particle temperature (T_α), and magnetic field measurements ($|B|$) from *Wind*/3DP and *Wind*/SWE. For each case, if all the data are available, the formula for the thermal pressure is taken as $P_{th} = N_i \times k \times T_i + N_e \times k \times T_e + N_\alpha \times k \times T_\alpha$, if the electron data are not available, the formula is alternatively taken as $P_{th} = 2N_i \times k \times T_i + N_\alpha \times k \times T_\alpha$. From July 2008 to June 2009, there are 29 days without electron data.

Figure 8 shows a histogram of the relative total pressure changes, dP_t/P_{t1}, during the deep solar minimum, where P_{t1} is the total pressure before the DPP event, P_{t2} is the total pressure after the event, and $dP_t = |P_{t2} - P_{t1}|$. In more than 76.7 % of the events, the relative total pressure change across the event is less than 10 %, which can be taken as evidence of structures with pressure balance (PBSs, Riazantseva *et al.* 2005a; 2005b); for about 7.6 % of the events, the relative total pressure changes by more than 30 %. It should be pointed out that during the previous solar minimum, electron data are available for less than half of the time (155 days); therefore, pressure balance comparisons between the two recent solar minima have not been done.

For most of the events, the PBSs may be tangential discontinuities. Thus far, the categories of small-scale solar wind structures have been poorly investigated. Riazantseva, Zastenker, and Richardson (2005) attempted to preliminarily classify the types of large and sharp solar wind ion flux changes observed by *Interball-1* from 1996 to 1999. Of the 207 events they studied, about 5 % were rotational discontinuities, nearly 50 % were tangential discontinuities, and the remaining 45 % of the events could not be classified unambiguously as any known discontinuity. A more detailed analysis to classify the observed DPPs by discontinuity type, which should help to explain the nature and origin of these structures, will be conducted in our future work.

Table 2 Number of DPPs associated with large-scale solar wind transients during the recent two solar minima. Some DPPs are associated with more than one type of large-scale transient.

Solar minimum	Solar min. 23 – 24	Solar min. 22 – 23
No. of SIRs	41	42
No. of ICMEs	8	4
No. of SIR-related DPPs[a]	184 (81.4 %)	365 (49.9 %)
No. of ICME-related DPPs[b]	25 (11.1 %)	23 (3.1 %)
No. of SIR- and ICME-related DPPs	13 (5.8 %)	16 (2.2 %)
No. of DPPs not associated with LSSWTs[c]	30 (13.3 %)	360 (49.2)

[a]DPPs that are only associated with SIRs and are associated with both ICMEs and SIRs are 6 included.

[b]DPPs that are only associated with ICMEs and are associated with both ICMEs and SIRs are 8 included.

[c]LSSWTs: large-scale solar wind transients.

Because some events are not in pressure balance, these structures must evolve with time. For example, Zastenker and Riazantseva (2007, 2008), Dalin *et al.* (2008), Rakhmanova, Riazantseva, and Zastenker (2012) used the coordinated observations of several spacecraft to investigate the dynamics of the sharp fronts of solar wind changes and found significant steepening of these sharp plasma changes up to around a million of kilometers.

3.3. Association with Large-Scale Solar Wind Transients

As shown in Figure 2, DPPs appear in groups in the solar wind. Dalin *et al.* (2002) suggested that the creation of sharp and large pressure changes might require that special conditions exist in the solar wind. Therefore, which type of solar wind the DPPs prefer to reside in is an interesting problem that might be related to their origins.

There is a tendency that the number of DPPs for days when solar wind transients, including ICMEs and SIRs, are observed is usually larger, as seen from Figure 2. Moreover, the continuous "active" days when DPPs are observed sequentially as in a pulse packet lasting 2 – 3 days are mainly associated with passages of ICMEs or SIRs. Here, we attempt to determine quantitatively the association of DPPs with these large-scale structures. The start time and the end time of ICME and SIR passages for July 2008 – June 2009 are obtained from publicly available catalogues compiled by Jian Lan (http://www-ssc.igpp.ucla.edu/~jlan/ACE/Level3/SIR_List_from_Lan_Jian.pdf and http://www-ssc.igpp.ucla.edu/~jlan/ACE/Level3/ICME_List_from_Lan_Jian.pdf). In this study, a DPP event is considered to be associated with an ICME or SIR if it occurs within the time interval of their passages.

During the deep solar minimum, eight ICMEs and 41 SIRs are detected according to the two lists. However, if we consider the availability of 3DP data during this period, the number reduces to seven ICMEs and 37 SIRs. The numbers of DPPs associated with the large-scale transients of each solar minimum are listed in Table 2. During the deep minimum, 184 cases are identified as SIR-related DPPs; that is, 81.4 % of 226 cases are located within SIRs. In addition, 25 cases, or 11.1 %, are identified as ICME-related DPPs. Only 30 cases, or 13.3 %, show no association. It should be noted that these large-scale structures show partial overlap in some cases. Thus, there are DPPs related to more than one type of large-scale transient. During this period, 13 cases, or 5.8 %, are SIR- and ICME-related DPPs. To summarize, an overwhelming majority of DPPs, 86.7 % of all 226 cases, are associated with SIRs or ICMEs

Table 3 Comparison of DPP parameters for the two recent solar minima.

Solar min.	Period	No. of DPPs	No. of obs. days	Frequency [*per* day]	$\langle \lvert dP \rvert \rangle$ [nPa]
22 – 23	1996	732	366	2.0	1.64
23 – 24	July 2008 – June 2009	226	322[a]	0.7	1.52

Solar min.	Period	$\langle \lvert dP \rvert / P_{av} \rangle$	$\langle (dP/P_{av})/(dN/N_{av}) \rangle$	$\langle dV \rangle$ [km s^{-1}]	$\langle dT \rangle$ [s]
22 – 23	1996	0.43	1.15	13	173
23 – 24	July 2008 – June 2009	0.44	1.13	12	171

[a]During the 1-year period (365 days) from July 2008 to June 2009, 3DP data are not available for 43 days.

during the deep solar minimum. That is, ICMEs and SIRs provide favorable conditions for the origin and propagation of DPPs during the deep solar minimum.

For the previous solar minimum, there are four ICMEs and 42 CIRs. Among the 732 DPPs that occur during 1996: 3.1 % are ICME-related, 49.9 % are CIR-related, and 2.2 % are associated with both SIRs and ICMEs. That is, 50.8 % of the DPPs of the solar minimum between Cycles 22 and 23 are associated with large-scale solar wind transients. Although the numbers and properties of ICMEs and CIRs differ little during the two minima (Jian, Russell, and Luhmann, 2011), the percentage of DPPs associated with large-scale solar wind transients of the deep solar minimum is significantly larger than that of the previous solar minimum.

4. Discussion

In the previous section, we have compared the statistical results of DPP properties for the deep solar minimum and the previous solar minimum. The key parameters of DPPs during the two recent solar minima are summarized in Table 3. In this table, the first and second columns specify the two time intervals surveyed. In the upper half of Table 3, the third to fifth columns show the number of DPPs, observation days and the frequency of DPPs *per* day during each solar minimum; the remaining columns show average values of key parameters of the DPPs. In summary, there are many properties in common for the DPPs during the two minima: 1) The distributions of $|dP|$ peak at 1.0 – 1.5 nPa. 2) The most probable relative pressure changes are 0.2 – 0.8. 3) The durations of DPPs show a broad peak between 150 s and 240 s with a mean of about 170 s. 4) The distributions and average values of absolute and relative amplitude of the dynamic pressure changes and DPPs durations are similar. 5) The dynamic pressure changes across DPPs are dominated by density changes and the role of the velocity variation is rather small. 6) The majority of DPPs are related to large-scale solar wind transients.

By comparison,we find that there are two impressive features for the DPPs that occurred during the deep solar minimum: 1) A dominant portion of DPPs, 86.7 %, are associated with large-scale solar wind transients; DPPs are more closely associated with disturbed large-scale solar wind structures than undisturbed quiet solar wind. 2) The average occurrence frequency of DPPs during the deep solar minimum is abnormally low.

The distributions of solar wind proton density, speed, and dynamic pressure for the two solar minima are determined using the 93-s time resolution data from *Wind*/SWE and are

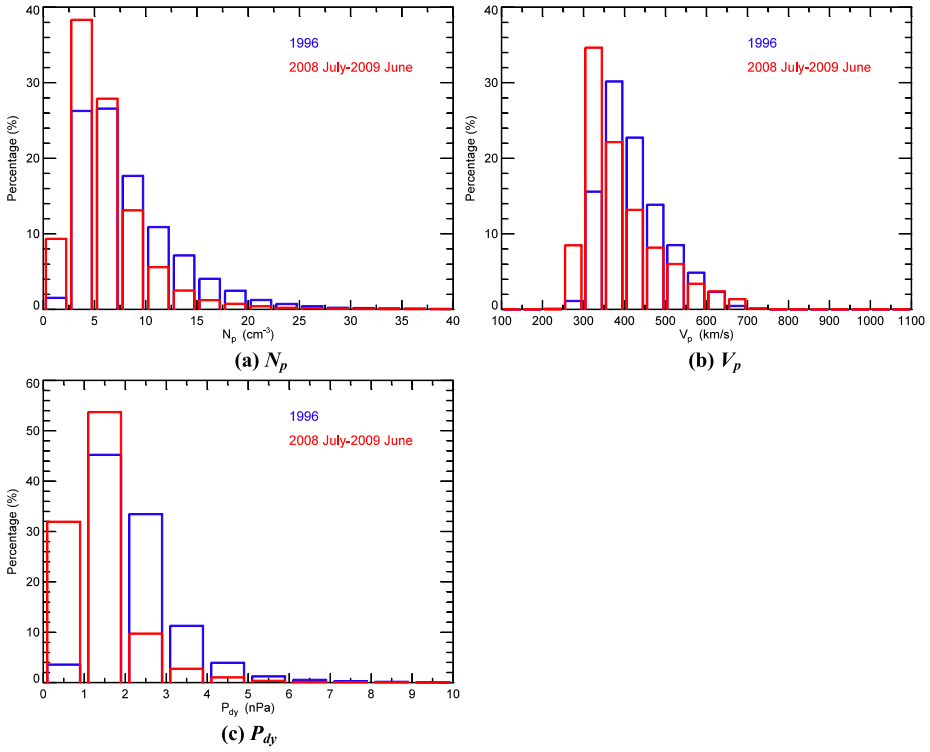

Figure 9 Histograms of (a) solar wind proton density, (b) speed, and (c) dynamic pressure for the solar minimum between Cycles 23 and 24 (red) and 22 and 23 (blue).

Table 4 Comparison of key solar wind parameters for the two solar minima.

Solar min.	$\langle V_{\rm p}\rangle$ [km s^{-1}]	$\langle N_{\rm p}\rangle$ [cm^{-3}]	$\langle P_{\rm dy}\rangle$ [nPa]	$\delta_{\rm Pdy}$ [nPa]	$CV_{\rm Pdy}$
22 – 23	422	8.4	2.29	2.45	107 %
23 – 24	390	6.1	1.42	1.37	96 %

shown in Figure 9. As can be seen from Figure 9a–b, the deep minimum has the slower and less dense solar wind in comparison with the previous minimum. The slower solar wind speed and lower proton density then jointly lead to weaker dynamic pressure as shown in Figure 9c. In addition, the averages of solar wind proton speed, density, and dynamic pressure for the two considered periods are listed in Table 4 (third to fifth columns). The average solar wind speed of the deep solar minimum is only 390 km s^{-1}, which is 7.6 % slower than the 422 km s^{-1} recorded during the previous minimum. The average proton density of the deep solar minimum is 6.1 cm^{-3}, which is less than 73 % of the 8.4 cm^{-3} recorded during the previous minimum. Due to the slower speed and lower density, the average dynamic pressure of the solar minimum between Cycles 23 and 24 is only 1.42 nPa, which is 38 % weaker than the 2.29 nPa recorded during the solar minimum between Cycles 22 and 23.

The standard deviations ($\delta_{\rm Pdy}$) of the solar wind dynamic pressure during the deep minimum and the previous minimum are 1.37 and 2.45, respectively (Table 4). The coefficient

of variation (CV_{Pdy}, also known as "relative variability", which is equal to the standard deviation of a distribution divided by its mean) of the solar wind dynamic pressure during the deep minimum is 96 %, which is smaller than the 107 % recorded during the previous solar minimum (Table 4). Thus, it can be concluded that the solar wind dynamic pressure fluctuation or variability of the deep minimum is significantly weaker than that of the previous minimum.

The selection criteria of DPPs demand that the dynamic pressure change should exceed 1 nPa across the transition region. Due to the abnormally lower dynamic pressure and weaker dynamic pressure variability, this requirement is more difficult to satisfy for the deep solar minimum. This may be the reason why fewer DPPs are recorded during this special period compared with the previous solar minimum. The solar minimum-to-minimum differences in the number of DPPs and occurrence rate also imply that the annual distribution of DPPs may have a solar cycle dependence and that a higher degree of solar activity may result in a higher DPP occurrence rate.

5. Conclusions

During the deep solar minimum between Solar Cycles 23 and 24, 1 year (1 July 2008 – 30 June 2009) of solar wind data were surveyed to construct a dataset of DPP events for our statistical study. During this period, 226 DPPs occurred with a frequency of 0.7 events *per* day. These dynamic pressure changes are not distributed homogeneously in time but are observed to occur in clumps. In addition, the pressure changes are mainly dominated by density changes, the role of the velocity change in these pressure changes is rather small. The average absolute dynamic pressure change is 1.52 nPa, the average value of the relative pressure change is 0.44, and their average duration is 171 s. About 76.7 % of the events are considered as pressure balance structures. In addition, in 7.6 % of the events, the relative total pressure change is more than 30 %. When there is no pressure balance, the events should evolve.

It is found that the number and the average frequency of DPPs during the deep solar minimum are only about one-third of those during the previous minimum. The solar minimum-to-minimum differences of the number of DPPs and occurrence rate also imply that the annual distribution of DPPs has a solar cycle dependence. From a statistical perspective, other basic properties of DPPs, such as absolute and relative amplitude of the dynamic pressure changes and durations, do not show obvious differences between the two solar minima. Therefore, such parameters may not be cycle dependent.

Furthermore, an overwhelming majority of DPPs during the deep solar minimum, 86.7 %, is associated with large-scale solar wind transients. Since the deep minimum has the weaker and less variable solar wind dynamic pressure in comparison with the previous solar minimum, DPPs with large dynamic pressure changes in the undisturbed solar wind are less frequently detected.

Acknowledgements This work is jointly supported by the National Natural Science Foundation of China (41304146, 41174152, 41374188, 41231068), and the Specialized Research Fund for State Key Laboratories. We thank NASA/GSFC for the use of the key parameters from *Wind* obtained *via* the CDA Web page.

References

Araujo-Pradere, E.A., Redmon, R., Fedrizzi, M., Viereck, R., Fuller-Rowell, T.J.: 2011, Some characteristics of the ionospheric behavior during the solar cycle 23 – 24 minimum. *Solar Phys.* **274**, 439. DOI.

Barkhatov, N.A., Korolev, A.V., Zastenker, G.N., Ryazantseva, M.O., Dalin, P.A.: 2003, MHD simulations of the dynamics of sharp disturbances of the interplanetary medium and comparison with spacecraft observations. *Cosm. Res.* **41**, 529. DOI.

Borodkova, N.L., Zastenker, G.N., Riazantseva, O., Richardson, J.D.: 2005, Large and sharp solar wind dynamic pressure variations as a source of geomagnetic field disturbances at the geosynchronous orbits. *Planet. Space Sci.* **53**, 25. DOI.

Chen, Y., Liu, L., Wan, W.: 2011, Does the F10.7 index correctly describe solar EUV flux during the deep solar minimum of 2007 – 2009? *J. Geophys. Res.* **116**, A04304. DOI.

Dalin, P.A., Zastenker, G.N., Paularena, K.I., Richardson, J.D.: 2002, A survey of large, rapid solar wind dynamic pressure changes observed by Interball-1 and IMP 8. *Ann. Geophys.* **20**, 293. DOI.

Dalin, P.A., Yermolaev, Yu.I., Zastenker, G.N., Riazantseva, M.O.: 2008, Large-scale solar wind density enhancement and its boundaries: Helios 1, 2 and IMP 8 observations. *Planet. Space Sci.* **56**, 398. DOI.

Emmert, J.T., Lean, J.L., Picone, J.M.: 2010, Record-low thermospheric density during the 2008 solar minimum. *Geophys. Res. Lett.* **37**, L12102. DOI.

Gibson, S.E., Kozyra, J.U., de Toma, G., Emery, B.A., Onsager, T., Thompson, B.J.: 2009, If the Sun is so quiet, why is the Earth ringing? A comparison of two solar minimum intervals. *J. Geophys. Res.* **114**, A09105. DOI.

Heelis, R.A., Coley, W.R., Burrell, A.G., Hairston, M.R., Earle, G.D., Perdue, M.D., Power, R.A., Harmon, L.L., Holt, B.J., Lippincott, C.R.: 2009, Behavior of the O^+/H^+ transition height during the extreme solar minimum of 2008. *Geophys. Res. Lett.* **36**, L00C03. DOI.

Jian, L., Russell, C.T., Luhmann, J.G.: 2011, Comparing solar minimum 23/24 with historical solar wind records at 1 AU. *Solar Phys.* **274**, 321. DOI.

Khabarova, O.V., Zastenker, G.N.: 2011, Sharp changes of solar wind ion flux and density within and outside current sheets. *Solar Phys.* **270**, 311. DOI.

Kilpua, E.K.J., Jian, L., Li, Y., Luhmann, J.G., Russell, C.T.: 2012, Observations of ICMEs and ICME-like solar wind structures from 2007 – 2010 Using near-Earth and STEREO observations. *Solar Phys.* **281**, 391. DOI.

Liu, L., Chen, Y., Le, H., Kurkin, V.I., Polekh, N.M., Lee, C.-C.: 2011, The ionosphere under extremely prolonged low solar activity. *J. Geophys. Res.* **116**, A04320. DOI.

Liu, L., Yang, J., Le, H., Chen, Y., Wan, W., Lee, C.-C.: 2012, Comparative study of the equatorial ionosphere over Jicamarca during recent two solar minima. *J. Geophys. Res.* **117**, A01315. DOI.

Lühr, H., Xiong, C.: 2010, The IRI-2007 model overestimates electron density during the 23/24 solar minimum. *Geophys. Res. Lett.* **37**, L23101. DOI.

Moore, T.E., Fok, M.-C., Delcourt, D.C., Slinker, S.P., Fedder, J.A.: 2007, Global aspects of solar wind-ionosphere interactions. *J. Atmos. Solar-Terr. Phys.* **69**, 265. DOI.

Motoba, T., Fujita, S., Kikuchi, T., Tanaka, T.: 2007, Solar wind dynamic pressure forced oscillation of the magnetosphere-ionosphere coupling system: A numerical simulation of directly pressure-forced geomagnetic pulsations. *J. Geophys. Res.* **112**, A11204. DOI.

Parkhomov, V.A., Riazantseva, M.O., Zastenker, G.N.: 2005, Local amplification of auroral electrojet as response to sharp solar wind dynamic pressure change on June 26 1998. *Planet. Space Sci.* **53**, 265. DOI.

Rakhmanova, L.S., Riazantseva, M.O., Zastenker, G.N.: 2012, Dynamics of the small-scale solar wind structures with sharp boundaries under transfer from the solar wind to magnetosheath. In: Šafránková, J., Pavlů, J. (eds.) *WDS 2012, Proc. 21st Ann. Conf. Doctoral Students, Part II*, 176.

Riazantseva, M.O., Zastenker, G.N., Richardson, J.D.: 2005, The characteristics of sharp (small-scale) boundaries of solar wind plasma and magnetic field structures. *Adv. Space Res.* **35**, 2147. DOI.

Riazantseva, M.O., Dalin, P.A., Zastenker, G.N., Richardson, J.D.: 2003a, Orientation of sharp fronts in the solar wind plasma. *Cosm. Res.* **41**, 382.

Riazantseva, M.O., Dalin, P.A., Zastenker, G.N., Parhomov, V.A., Eselevich, V.G., Eselevich, M.V., Richardson, J.D.: 2003b, Properties of sharp and large changes in the solar wind ion flux (density). *Cosm. Res.* **41**, 371. DOI.

Riazantseva, M.O., Khabarova, O.V., Zastenker, G.N., Richardson, J.D.: 2005a, Sharp boundaries of solar wind plasma structures and an analysis of their pressure balance. *Cosm. Res.* **43**, 157. DOI.

Riazantseva, M.O., Zastenker, G.N., Richardson, J.D., Eiges, P.E.: 2005b, Sharp boundaries of small- and middle-scale solar wind structures. *J. Geophys. Res.* **110**, A12110. 2005. DOI.

Riazantseva, M.O., Khabarova, O.V., Zastenker, G.N., Richardson, J.D.: 2007, Sharp boundaries of the solar wind plasma structures and their relationship to solar wind turbulence. *Adv. Space Res.* **40**, 1802. DOI.

Russell, C.T., Jian, L.K., Luhmann, J.G.: 2013, How unprecedented a solar minimum was it? *J. Adv. Res.* **4**, 253. DOI.

Solomon, S.C., Woods, T.N., Didkovsky, L.V., Emmert, J.T., Qian, L.: 2010, Anomalously low solar extreme-ultraviolet irradiance and thermospheric density during solar minimum. *Geophys. Res. Lett.* **37**, L16103. DOI.

Solomon, S.C., Qian, L., Didkovsky, L.V., Viereck, R.A., Woods, T.N.: 2011, Causes of low thermospheric density during the 2007 – 2009 solar minimum. *J. Geophys. Res.* **116**, A00H07. DOI.

Yu, Y.-Q., Ridley, A.J.: 2011, Understanding the response of the ionosphere-magnetosphere system to sudden solar wind density increases. *J. Geophys. Res.* **116**, A04210. DOI.

Zastenker, G.N., Riazantseva, M.O.: 2007, Multipoint observations of the dynamics of the sharp solar wind structure boundaries. *Planet. Space Sci.* **55**, 2340. DOI.

Zastenker, G.N., Riazantseva, M.O.: 2008, Similarity and difference of the durations of the small-scale solar wind structure boundaries by multipoint observations. *J. Atmos. Solar-Terr. Phys.* **70**, 377. DOI.

Zuo, P.B., Feng, X.S., Xie, Y.Q., Wang, Y., Li, H.J., Xu, X.J.: 2015, Automatic detection algorithm of dynamic pressure pulses in the solar wind. *Astrophys. J.* **803**, 94. DOI.